



Endoderm and Hepatic Progenitor Cells Engraft in the Quiescent Liver Concurrent with Intrinsically Activated Epithelial-to-Mesenchymal Transition

Cell Transplantation
Volume 30: 1–12
© The Author(s) 2021
Article reuse guidelines:
sagepub.com/journals-permissions
DOI: 10.1177/0963689721993780
journals.sagepub.com/home/ct


W. Samuel Fagg^{1,2} , Naiyou Liu¹, Igor Patrikeev³, Omar A. Saldarriaga⁴, Massoud Motamedi⁵, Vsevolod L. Popov⁴, Heather L. Stevenson⁴, and Jeffrey H. Fair¹

Abstract

Stem cell transplantation to the liver is a promising therapeutic strategy for a variety of disorders. Hepatocyte transplantation has short-term efficacy but can be problematic due to portal hypertension, inflammation, and sinusoidal thrombosis. We have previously transplanted small mouse endoderm progenitor (EP) cells to successfully reverse a murine model of hemophilia B, and labeling these cells with iron nanoparticles renders them responsive to magnetic fields, which can be used to enhance engraftment. The mechanisms mediating progenitor cell migration from the sinusoidal space to the hepatocyte compartment are unknown. Here we find human EP and hepatic progenitor (HP) cells can be produced from human embryonic stem cells with high efficiency, and they also readily uptake iron nanoparticles. This provides a simple manner through which one can readily identify transplanted cells in vivo using electron microscopy, shortly after delivery. High resolution imaging shows progenitor cell morphologies consistent with epithelial-to-mesenchymal transition (EMT) mediating invasion into the hepatic parenchyma. This occurs in as little as 3 h, which is considerably faster than observed when hepatocytes are transplanted. We confirmed activated EMT in transplanted cells in vitro, as well as in vivo 24 h after transplantation. We conclude that EMT naturally occurs concurrent with EP and HP cell engraftment, which may mediate the rate, safety, and efficacy of early cell engraftment in the undamaged quiescent liver.

Keywords

liver, cell transplantation, stem cells, endoderm, regenerative medicine

Introduction

Cell transplantation to the liver is a potential alternative to solid organ transplant that may provide adjunctive, bridging, or replacement therapy to patients with metabolic disorders or liver failure^{1,2}. Hepatocyte transplantation has proven effective in temporary reversal of metabolic disorders in patients awaiting liver transplant, but is not without risk to the recipient due to a variety of factors³. One such issue is the mechanism through which hepatocytes engraft in the liver: studies in rats have elucidated this involves portal occlusion and inflammation⁴. Unfortunately this observation in a model organism was reproduced in the clinic and portal thrombosis lead to the death of a hepatocyte transplant recipient⁵. Despite further refinement, hepatocyte transplantation is primarily reserved for bridging therapy in patients awaiting liver transplant or for patients ineligible to receive a transplant^{6,7}.

¹ Transplant Division, Department of Surgery, University of Texas Medical Branch, Galveston, TX, USA

² Department of Biochemistry and Molecular Biology, University of Texas Medical Branch, Galveston, TX, USA

³ Department of Vice President for Research, University of Texas Medical Branch, Galveston, TX, USA

⁴ Department of Pathology, University of Texas Medical Branch, Galveston, TX, USA

⁵ Department of Ophthalmology, University of Texas Medical Branch, Galveston, TX, USA

Submitted: October 15, 2020. Revised: January 14, 2021. Accepted: January 15, 2021.

Corresponding Authors:

W. Samuel Fagg and Jeffrey H. Fair, Transplant Division, Department of Surgery, University of Texas Medical Branch, Galveston, TX 77555, USA.
Emails: wsfagg@utmb.edu; jhfair@utmb.edu



Basic and translational studies are currently underway to identify different cell types that can be safe and effective candidates for liver cell transplantation^{8–10}. While various types of human cells (stem/progenitor or otherwise) can be effective in disparate models of liver disease, most rely on some form of liver damage^{11–13}. This creates an inflamed and/or regenerative state within the organ, which is amenable to uptake, engraftment, and long-term dwell of transplanted cells. In the case of most metabolic disorder patients, the liver is otherwise structurally normal, and any reduction of function could have deleterious effects. This may preclude the patient population in greatest need of bridging therapy from being cell transplant candidates.

We have used mixed populations of mouse endoderm progenitor (EP) cells to overcome this caveat, and observed long-term engraftment and reversal of hemophilia B phenotype in factor IX^{-/-} mice, independent of preconditioning liver damage¹⁴. Further studies indicated labeling these cells with supraparamagnetic particles (SPMs) and magnetic targeting enhanced retention in the undamaged liver parenchyma, significantly increasing overall engraftment¹⁵. Interestingly, a comparable human cell was observed 42 days post-transplant in an immunocompromised mouse model, independent of liver damage¹⁶, so the use of a human progenitor cell may also be effective. The mechanism through which these EP-like cells engraft, however, is unknown.

The above examples of EP cells capable of engraftment and long-term dwell in the undamaged liver show similar lineage commitment and gene expression characteristics. Additionally, these cells are all intrinsically biased toward epithelial-to-mesenchymal transition (EMT), which mediates migration and invasion through a substrate. The process is observed in both the mouse embryo, as cells migrating the primitive streak ultimately become definitive endoderm and mesoderm^{17,18}, and in human embryonic stem cell (hESC)-derived EP and hepatic progenitor (HP) cells¹⁹. Taking these observations along with the smaller cell size of EP and HP cells compared to hepatocytes (approximately 40 μm), we hypothesized EMT may be an active process in early engraftment during cell transplantation to the liver. This may effectively reduce the potential of portal emboli and the time required for transplanted cells to migrate through the space of Disse and integrate into the parenchyma, each of which could potentially reduce inflammation and other complications in the recipient.

Here we address the question of whether human EP and HP cells have early liver engraftment characteristics that correlate with and may be enhanced by EMT. Using recent differentiation strategies, we find EP and HP cells can be produced at very high efficiency, and that SPM labeling of these cells facilitates imaging by electron microscopy (EM). The use of high resolution imaging of EP and HP cells shortly after transplantation shows the morphologic characteristics of EMT *in vivo*, and anatomically we find these cells incorporated into the parenchyma in as few as 3 h post-

transplant. Additionally, using immunolabeling along with SPM-based imaging, we observe transplanted HP cells with active EMT migrating through the undamaged liver 24 h after delivery. These observations support a model of early cell engraftment in which EP and HP cells use active migration mechanisms to efficiently integrate into the parenchyma. These processes may represent a safety advantage over previously described mechanisms of hepatocyte engraftment that have led to adverse events.

Materials and Methods

Cell Culture and Differentiation

We used H9 hESCs that express humanized renilla Green Fluorescent Protein (hrGFP) localized to the nucleus (a kind gift from Seigo Hatada²⁰) cultured in feeder-free conditions on hESC-qualified Matrigel (Corning, Corning, NY, USA) using mTeSR1 Media (Stemcell Technologies, Vancouver, Canada). For differentiation experiments, ~50% plate density of cells was passed using ReLeSR or Gentle Cell Dissociation Reagent (both Stemcell Technologies) at an approximate ratio of 1:5 and allowed to equilibrate in mTeSR1 for 1 to 2 days prior to differentiation. The differentiation of H9 human stem cells to endodermal and HP cells¹³ was performed as described, as were the procedures to make cardiac mesoderm²¹ and ectoderm²² but using CDM2 as the basal media for 3 days then an additional 4 days with CDM2 including 10% knockout serum replacement (Thermo Fisher; Waltham, MA, USA).

RNA Extraction and Reverse Transcription-quantitative Polymerase Chain Reaction

Real-time fluorescent quantitative polymerase chain reaction was performed as described previously¹⁵. Total RNA was harvested and purified using the ReliaPrep RNA Mini-Prep System (Promega, Madison, WI, USA). Either 0.5 or 1 μg was reverse transcribed using the SuperScript III reverse transcription kit (Thermo Fisher) following the manufacturer's directions. The product cDNA template was diluted 25- to 50-fold and amplified using SYBR Green qPCR Master Mix (Thermo Fisher) on an ABI 7300 optical thermocycler (Applied Biosystems/Thermo Fisher). We performed melt curve analysis for every reaction, and included a no template control to verify specific amplification was template-dependent. Data were analyzed using the delta-delta CT method and reported as relative to HMBS, which was used as the internal control/"housekeeping" gene. The primer sequences were used for Hydroxymethylbilane Synthase (HMBS) (forward: 5'-GGAGCCATGTCTG GTAACGG-3', reverse: 5'-CCACGCGAATCACTCTCA TCT-3'), OCT4 (forward: 5'-AGTGAGAGGCAACCTG GAGA-3', reverse: 5'-ACACTCGGACCACATCCTTC-3'), SOX2 (forward: 5'-TGGACAGTTACGCGCACAT-3', reverse: 5'-CGAGTAGGACATGCTGTAGGT-3'), SOX17

(forward: 5'-CGCACGGAATTTGAACAGTA-3', reverse: 5'-GGATCAGGGACCTGTCACAC-3'), FOXA2 (forward: 5'-GGGAGCGGTGAAGATGGA-3', reverse: 5'-TCATGT TGCTACGGAGGAGTA-3'), AFP (forward: 5'-CTTTG GGCTGCTCGCTATGA-3', reverse: 5'-GCATGTTGATTT AACAAGCTGCT-3'), NCAD (forward: 5'-CAACGGGGA CTGCACAGATG-3', reverse: 5'-TGTTTGGCCTGGCG TTCTTT-3'), ECAD (forward: 5'-AGCCCTTACTGCC CCAGAG-3', reverse: 5'-GGGAAGATACCGGGGAC AC-3'), and SNAI1 (forward: 5'-CCGACCCCAATCGG AAGCCTAACT-3', reverse: 5'-AGTCCCAGATGAG CATTGGCAGCGAG-3').

Immunofluorescence

In vitro cell-based immunofluorescent staining was performed according to previously established protocols²³. The cells were incubated with primary antibodies at concentration recommended by the manufacturers: primary antibodies included mouse anti-SOX2 (catalog # 4900 S, Cell Signaling Technologies, Danvers, MA, USA) at 1:400 dilution, rat anti-SSEA3 (catalog # MAB-1434, R&D Systems, Minneapolis, MN, USA) at 10 µg/ml final concentration, goat anti-SOX17 (catalog # AF1924, R&D Systems) at 1:500 dilution, rabbit anti-AFP (catalog # SAB3500533, Sigma-Aldrich, St. Louis, MO, USA) at 1:200 dilution, mouse anti-NCAD (ab98952, Abcam, Cambridge, UK) at 1:500 dilution, and rabbit anti-ECAD (ab40772, Abcam) at 1:100 dilution. The applied secondary antibodies were all AlexaFlour (Thermo Fisher) at concentrations of 1 µg/ml: 568 goat anti-rabbit IgG (H + L) catalog # A11011, 647 goat anti-mouse IgG (H + L) catalog # A21235, 647 donkey anti-goat IgG (H + L) catalog # A21447, and 647 goat anti-rat (µ chain) catalog # A21248. Imaging was performed using either the Opera Phenix (PerkinElmer, Waltham, MA, USA; see Fig. 1B) or Olympus IX71 inverted fluorescence microscope (Olympus, Shinjuku City, Tokyo, Japan; see Figs. 2A, C and 4B).

Flow Cytometry

Cells were removed from plates/dishes by scraping into phosphate buffered saline (PBS), then an equal volume of Accu-max (Innovative Cell Technologies Inc., San Diego, CA, USA) was added. This was incubated 5 to 10 min at room temperature, at which time dissociation to a single cell suspension was verified by microscopy. Surface marker staining was performed to identify CXCR4 and CD99 positive cells following the manufacturer's instructions. The antibodies used were APC mouse anti-human CD184 (CXCR4; clone 12G5, BioLegend, San Diego, CA, USA), APC mouse anti-human CD99 (clone HCD99, BioLegend), or APC Mouse IgG_{2a}, k isotype control (catalog # 400222, BioLegend). After staining and washing, the cells were passed through a 40 µm strainer and kept on ice in the dark before analysis with BD FACS Aria IIU (Beckton Dickinson, Franklin Lakes, NJ,

USA) with assistance from the core facility operator. Data were analyzed using FlowJo software.

Western Blotting

Total protein was extracted using RSB100 buffer as previously described²⁴. Electrophoresis of denatured samples was conducted with Tris-glycine buffered sodium dodecyl sulfate polyacrylamide gel electrophoresis at 130 V for 1.5 h and proteins were then transferred at 90 V for 1 h by wet transfer to a nitrocellulose membrane. The membrane was blocked with 5% milk in tris-buffered saline (TBS) at room temperature for 1 h, then primary antibodies mouse anti-EOMES (clone 644730/catalog # MAB6166, R&D Systems), goat anti-SOX17 (catalog # AF1924, R&D Systems), rabbit anti-NKX2.5, rabbit anti-AFP (catalog # SAB3500533, Sigma-Aldrich), and rabbit anti-Tubulin (catalog # 2148 S, Cell Signaling Technologies) were used to probe for the specified antigen overnight at 4°C. Membranes were washed three times in TBS with 0.1% Tween-20 (TBST) and probed with infrared dye-conjugated secondary antibodies, all from LI-COR (Lincoln, NE, USA): IRDye 800CW donkey anti-rabbit IgG (1:15,000 dilution; catalog # 926-32213), IRDye 680RD donkey anti-goat IgG (1:20,000 dilution; catalog # 926-68074), or IRDye 680RD donkey anti-mouse IgG (1:20,000 dilution; catalog # 926-68072), then washed three additional times with TBST. Proteins were visualized by scanning on the Odyssey CLx system (LI-COR).

Superparamagnetic Microsphere (SPM) Labeling of EP and HP Cells

Cells were labeled with fluorescent (flash red)-conjugate SPM particles (0.9 µm diameter; Bangs Laboratories, Fishers, IN, USA) by incubation in cell culture for 18 h. Successful labeling was confirmed by fluorescent microscopy to visualize flash-red fluorescent signal.

Animals and Cell Transplantation

Wild-type C57/bl6 mice were obtained from Jackson Laboratory and housed in the Animal Resource Center Facility at the University of Texas Medical Branch (UTMB). All mice used were between 8 and 15 weeks age and weighed between 20 and 30 g. Mice were maintained on standard chow and kept on a 12-h light/dark cycle. All procedures performed were approved by the UTMB Institutional Animal Care and Usage Committee in compliance with the guidelines for humane care of laboratory animals.

For cell transplantation, EP or HP cells are detached using 0.25% trypsin 1 mM ethylenediaminetetraacetic acid (Thermo Fisher), then cells are counted, and diluted to the desired density in transplant buffer [1× PBS (Thermo Fisher) with 2% knockout serum replacement (Thermo Fisher) and 10 µg/ml DNase I (Thermo Fisher)]

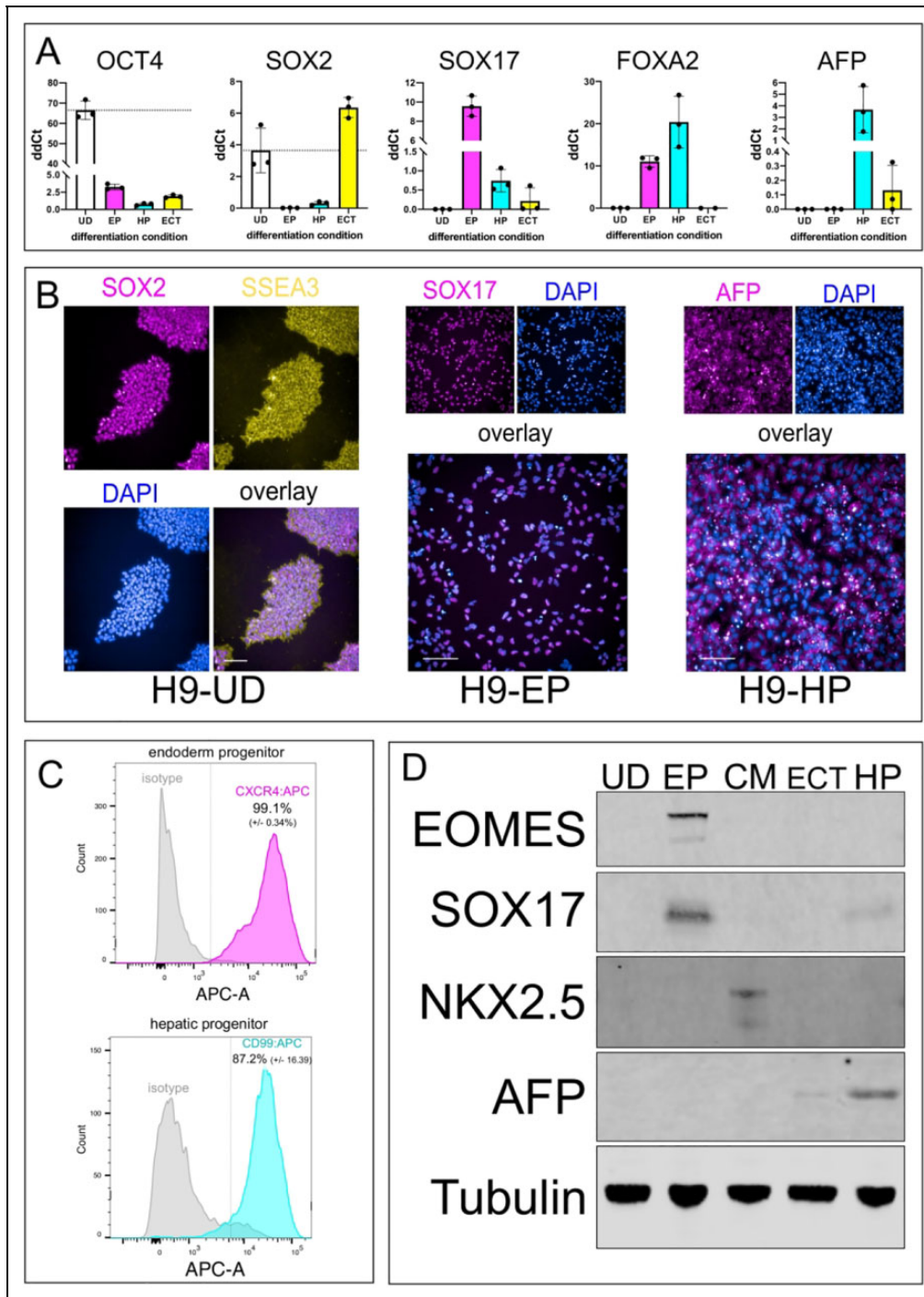


Figure 1. Human pluripotent stem cells efficiently form endoderm and hepatic progenitor cells in vitro. (A) RT-qPCR analysis of RNA extracted from UD, EP, HP, and ectoderm (ECT) cells displayed as delta-delta Ct values relative to HMBS “housekeeping gene product” ($n = 3$ biological replicates shown as individual points, bars show mean, and error bars show standard deviation). (B) Representative images of indirect immunofluorescence of UD H9 ESCs showing SOX2 (magenta), SSEA3 (yellow), DAPI (blue), and each channel overlaid; of EP cells showing SOX17 (magenta), DAPI (blue), and the two channels overlaid; and HP cells with AFP (magenta), DAPI (blue), and each channel overlaid. Scale bar denotes 100 μm . (C) Flow cytometry analysis of EP cells (top) stained with either isotype control antibody: APC conjugate (gray histogram) or anti-CXCR4: APC conjugate (magenta histogram), and HP cells (bottom) stained with either isotype control antibody: APC conjugate (gray histogram) or anti-CD99: APC conjugate (cyan histogram). Histograms show a result representative from four biological replicates; mean values for percent positive are shown \pm standard deviation. (D) Western blot analysis of total protein extracted from UD, EP, CM, ECT, or HP cells and probed with antibodies directed against EOMES, SOX17, NKX2.5, AFP, and Tubulin; results shown are representative of at least two biological replicates. CM: cardiac mesoderm; DAPI: 4',6-diamidino-2-phenylindole; EP: endoderm progenitor; HP: hepatic progenitor; UD: undifferentiated hESCs.

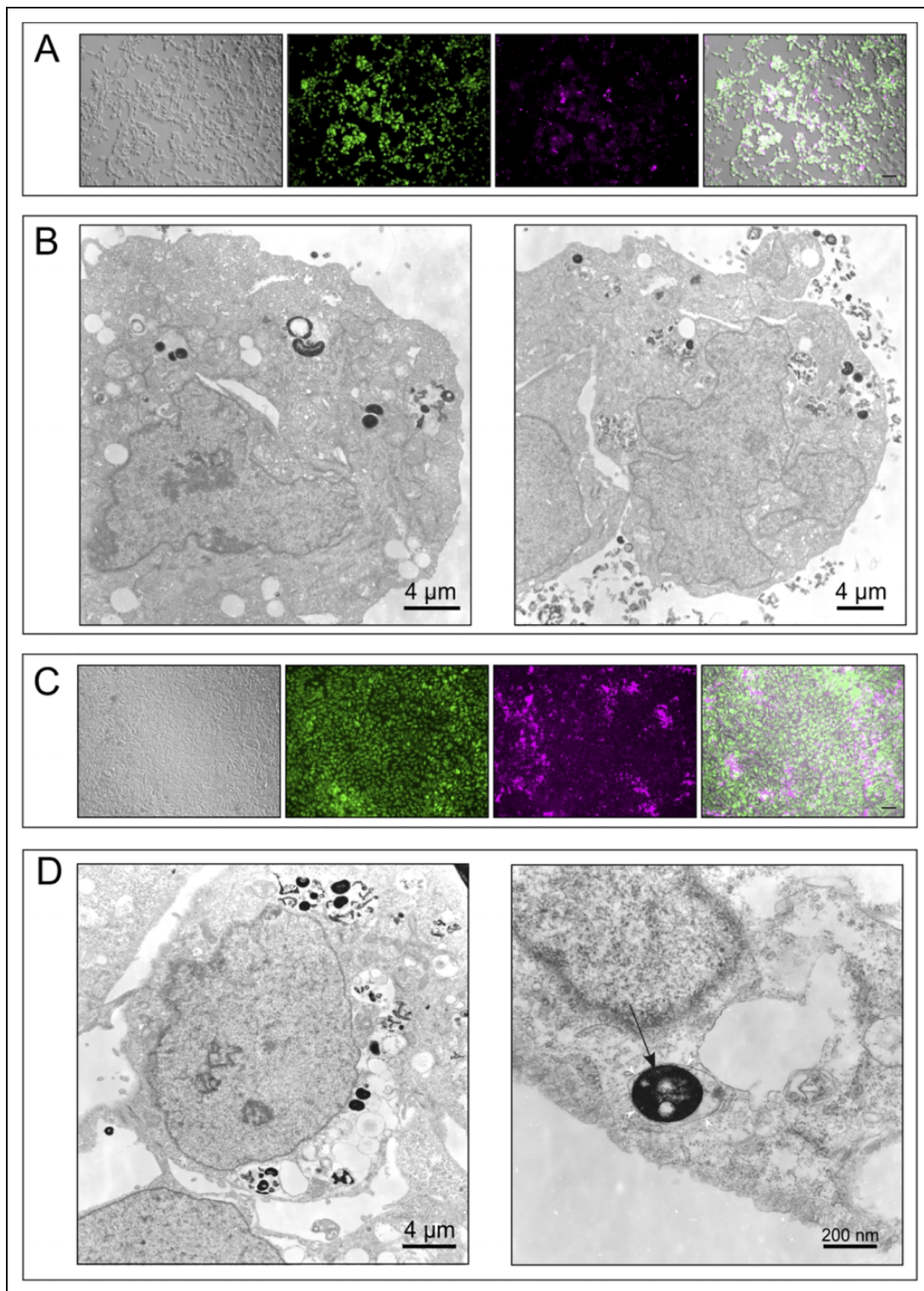


Figure 2. Human EP and HP cells readily endocytose SPM particles in vitro. (A) Representative result from live imaging of human EP cells with phase contrast (gray) and fluorescent imaging of nuclear-localized hrGFP (green), SPM-flash-red conjugate, and resulting overlaid images. Scale bar denotes 50 μm . (B) Electron microscopy showing two independent representative images of human EP cells shown in (A). Dark-staining objects are SPM particles; scale bar denotes 4 μm . (C) Representative result from live imaging of human HP cells with phase contrast (gray) and fluorescent imaging of nuclear-localized hrGFP (green), SPM-flash-red conjugate, and resulting overlaid images. Scale bar denotes 50 μm . (D) Electron microscopy showing two independent representative images of human HP. Dark-staining objects are SPM particles (indicated by black arrow in the image on right, while white arrowheads indicate membrane); scale bar denotes 4 μm (left) or 200 nm (right). EP: endoderm progenitor; HP: hepatic progenitor.

and kept on ice until transplant. The mice are prepared by anesthetization with isoflurane then making a 2 cm incision along the upper abdomen, and the dominant middle liver lobe is visualized. Either this lobe or the portal vein is injected manually with approximately 1 to 2 million cells (respectively), using a 32G needle. For parenchymal injections, after removal of the needle, gentle pressure is placed on the injection site for approximately 30 s, then the injection site is gently and minimally cauterized with battery operated cautery probe. For portal vein injections, Surgicel (Ethicon, Somerville, NJ, USA) is gently placed at the site of injection post-delivery and allowed to stop bleeding. The incision is then closed in two layers. The deep muscle layer is closed with running 5.0 vicryl, and the skin is closed with subcuticular sutures (6.0 coated Visorb). Just before finishing closure of the abdomen 1 ml of 37°C normal saline is instilled into the peritoneal cavity to aid rehydration along with dexmedetomidine at 1 mg/kg.

For *in vivo* imaging, mice were injected with d-Luciferin (150 mg/kg in PBS; PerkinElmer), anesthetized with isoflurane, and then imaged with the IVIS Spectrum Pre-clinical *In Vivo* Imaging System (PerkinElmer).

At the experimental endpoints, mice were anesthetized with isoflurane, then the abdomen was exposed by incision, followed by the thoracic cavity. The vascular system was thoroughly flushed with sterile PBS by delivery via injection to the portal vein or heart. The liver was then carefully removed, and each lobe was divided for RNA and DNA extraction (immediately frozen on dry ice), as well as for histological analysis. In the case of the latter (and see below for EM), the liver tissue was fixed in 10% formalin for 24 h then placed in 100% ethanol until being embedded in paraffin and 3 μ m sections were prepared by the UTMB Histology Core Facility. These were stained with Prussian blue and counterstained with eosin, essentially as described previously²⁵ and analyzed by light microscopy. For fluorescent imaging to identify transplanted EP and HP cells (that constitutively express nuclear localized hrGFP) in mouse livers, we used the Vectra 3 quantitative pathology imaging system (Akoya Biosciences, Hopkinton, MA, USA). Nuclei were counterstained with 4',6-diamidino-2-phenylindole (DAPI) and images were acquired using the Vectra multispectral camera configured to capture the spectrum from 420 to 520 nm to detect DAPI and green fluorescent protein (GFP).

Transmission Electron Microscopy

For ultrastructural analysis in ultrathin sections, small pieces (~1 mm³) of liver or cell monolayers were fixed for at least 1 h in a mixture of 2.5% formaldehyde prepared from paraformaldehyde powder, and 0.1% glutaraldehyde in 0.05 M cacodylate buffer pH 7.3 to which 0.1% picric acid (trinitrophenol) and 0.03% CaCl₂ were added. Then they were washed in 0.1 M cacodylate buffer and the cells were scraped off and processed further as a pellet. Then the samples were post-fixed in 1% OsO₄ in 0.1 M cacodylate buffer

pH 7.3 for 1 h, washed with distilled water, and en bloc stained with 2% aqueous uranyl acetate for 20 min at 60°C. The samples were dehydrated in ethanol, processed through propylene oxide, and embedded in Poly/Bed 812 (Polysciences, Warrington, PA, USA). Semi-thin sections 1 μ m thick were cut and stained with toluidine blue. Ultrathin sections were cut on Leica EM UC7 ultramicrotome (Leica Microsystems, Buffalo Grove, IL, USA), stained with lead citrate, and examined in a JEOL JEM-1400 transmission electron microscope at 80 kV. Images were acquired either on film or on bottom-mounted CCD camera Orius SC2001 (Gatan, Pleasanton, CA, USA).

Immunoelectron Microscopy

For post-embedding (on-section) immuno-gold EM the samples were fixed with the same primary aldehyde fixative but osmium fixation was omitted. The samples were stained en bloc with 2% aqueous uranyl acetate, dehydrated in 50% and 75% ethanol, and embedded in LR White resin medium grade (catalog # 14381-CA; Electron Microscopy Sciences, Hatfield, PA, USA). Ultrathin sections were cut on Leica EM UC7 ultramicrotome and collected onto Formvar-carbon coated nickel grids. The grids were incubated in a wet chamber sequentially on drops of blocking buffer [0.1% bovine serum albumin (BSA) and 0.01 M glycine in 0.05 M TBS], then on rabbit anti-Vimentin (ab92547; Abcam) primary antibody at (1:500) dilution in 1% BSA in 0.05 M TBS (diluting buffer) for 1 h at room temperature and then overnight at 4°C. After washing in blocking buffer grids were incubated with secondary antibody [goat anti-rabbit IgG (H + L)] conjugated to 15 nm colloidal gold particles (catalog # 25113, code815.011; Electron Microscopy Sciences), which was diluted 1:20 in diluting buffer, for 1 h at room temperature. After washing in TBS and distilled water grids were fixed in 2% aqueous glutaraldehyde, washed, stained with uranyl acetate and lead citrate, and examined in the transmission electron microscope.

Statistical Analysis

Results are shown as mean \pm standard deviation obtained from three independent biological replicates unless specified otherwise. In Fig. 4D, both the one-way analysis of variance and Mann-Whitney *U* test were implemented to measure statistical significance between two groups and both gave the same result. These were determined by analysis in Prism 8 software. Statistical significance was determined when *P* \leq 0.05 and is noted as such where applicable.

Results

hESCs Efficiently Differentiate to Endoderm and HP Cells

Prior to testing early human progenitor cells' early engraftment dynamics, we asked if previously reported high

efficiency differentiation to EP and HP cells could be reproduced¹³. Transcript abundance measurements indicated high levels of pluripotency marker OCT4 in undifferentiated hESCs (UD); likewise SOX2 levels were elevated in UD and ectoderm (Fig. 1A). Upon differentiation to EP and HP cells, these are reduced, while SOX17 (endoderm), FOXA2 (posterior foregut), and AFP (HP) abundance increased (Fig. 1A). We also observed this at the protein level: pluripotency markers SOX2 and SSEA3 are readily detectable in UD, while SOX17 and AFP are present in EP and HP cells, respectively (Fig. 1B). Additionally, flow cytometry analysis of EP and HP surface markers (CXCR4 and CD99, respectively) indicated differentiation efficiencies of 99.1% and 87.2%, respectively (Fig. 1C). Finally, population-level protein abundance measurement by western blot shows EOMES (mesendoderm/anterior primitive streak) and SOX17 proteins are present in EP cells; NKX2.5 is present in cardiac mesoderm cells but absent from UD, EP, and HP cells, and AFP protein is present in HP cells (Fig. 1D). Collectively, these data indicate EP and HP cells can be produced from UD hESCs at remarkably high efficiency, consistent with previous reports¹³.

Supraparamagnetic Particles are Readily Endocytosed and Visualized in EP and HP Cells

We used hESCs that constitutively express a nuclear-localized GFP variant (see Methods²⁰) in order to aid imaging in vitro and in vivo, and to ask if human progenitor cells can be labeled with SPMs with similar efficiencies to mouse EPs¹⁵. We found human EP cells are indeed readily labeled with flash-red conjugate SPMs (Fig. 2A). In order to verify the SPMs are indeed endocytosed, and not just associated externally with the plasma membrane, we performed EM on EP cells incubated overnight with SPMs. This approach indicated multiple SPMs are present in most EP cells visualized and appear to be enveloped within a membrane (Fig. 2B). We performed the same methods to test SPM labeling of HP cells and found similar results: immunofluorescence analysis indicated efficient labeling (Fig. 2C), while EM showed multiple SPMs endocytosed per cell (Fig. 2D). Importantly, higher resolution images indicated that SPMs are indeed membrane bound, confirming that the particles are endocytosed (Fig. 2D, right panel). We conclude that SPMs efficiently label human EP and HP cells, and thus may be useful for imaging early engraftment events in the quiescent liver.

SPM-labeled EP Cells are Readily Observed In Vivo

To determine if SPM-labeled human EP cells are indeed a reliable tool that we can use to visualize early engraftment in the quiescent liver at high resolution, we first performed in vivo analyses shortly (3 h) post-transplant. We confirmed the presence of transplanted EP cells using in vivo imaging (Fig. 3A), then collected liver samples for further analysis. Fluorescent imaging of liver sections allowed for

identification of nuclear hrGFP-expressing cells within the liver (Fig. 3B). Additionally, we used Prussian blue staining to identify SPM-labeled transplanted EP cells in vivo (Fig. 3C). These confirmatory results prompted us to conduct EM analysis, and we chose to focus initial efforts on the liver receiving human EP cells, as the murine equivalent has proven effective in our previous studies^{14,15}. We hypothesized SPM labeling could mediate high resolution visualization of very early engraftment events, and possibly elucidate how progenitor cells incorporate into the liver parenchyma. Indeed, we identify EP cells, identifiable by membrane-bound SPM, incorporated into the murine liver 3 h after transplant (Fig. 3D). Intriguingly, the EP cell shown is sub-endothelial and integrated into the hepatic parenchyma, with an apparent “leading edge” protruding between resident hepatocytes. This suggests an active invasion mechanism, by which the transplanted cell would have migrated through the space of Disse in a rapid manner. This is unique compared to the observed engraftment mechanism of hepatocytes, which are significantly larger cells and engraft via occlusion of the portal space, ultimately integrating into the sinusoid 16 to 20 h post-delivery⁴. We conclude SPM labeling is a simple method that is amenable to high resolution imaging by EM, and EP cells rapidly integrate into the hepatic parenchyma.

EMT is Intrinsically Activated in Human Endoderm and HP Cells

The above observations suggest a rapid, invasive mechanism through which EP cells engraft in the quiescent liver. The EMT is known to be an active process required for definitive endoderm and early HP cell specification, in both the mouse embryo²⁶ and hESCs differentiated in vitro¹⁹. Given these previous findings, we presumed EMT would also be active in the EP and HP cells we used for transplantation; however, the differentiation protocols we used are slightly different from previous reports. Thus, we assessed the cellular, molecular, and biochemical profiles of UD, EP, and HP cells to determine the extent to which EMT was active. Consistent with previous reports, we found elevated abundance of CDH2 (N-Cadherin) and reduced levels of CDH1 (E-Cadherin) transcripts in both EP and HP cells (Fig. 4A). Additionally, there was a greater than two-fold increase in SNAI1 transcript levels in EP cells (Fig. 4A). We also measured protein abundance of E-Cadherin and N-Cadherin in UD, EP, and HP cells. These analyses corroborated the transcript abundance measurements and indicated repression of EMT in UD cells, and activation of it in both EP and HP cells, as the ratio of N-Cadherin to E-Cadherin protein is elevated in the latter two types of cells (Fig. 4B). Interestingly, the mean ratio of N-Cadherin:E-Cadherin is higher in EP cells than in HP cells, although the difference is not significant. This suggests a wider range of EMT in the EP cells than in the HP cells, the latter of which may be primed to reverse the process upon further differentiation¹⁹. We

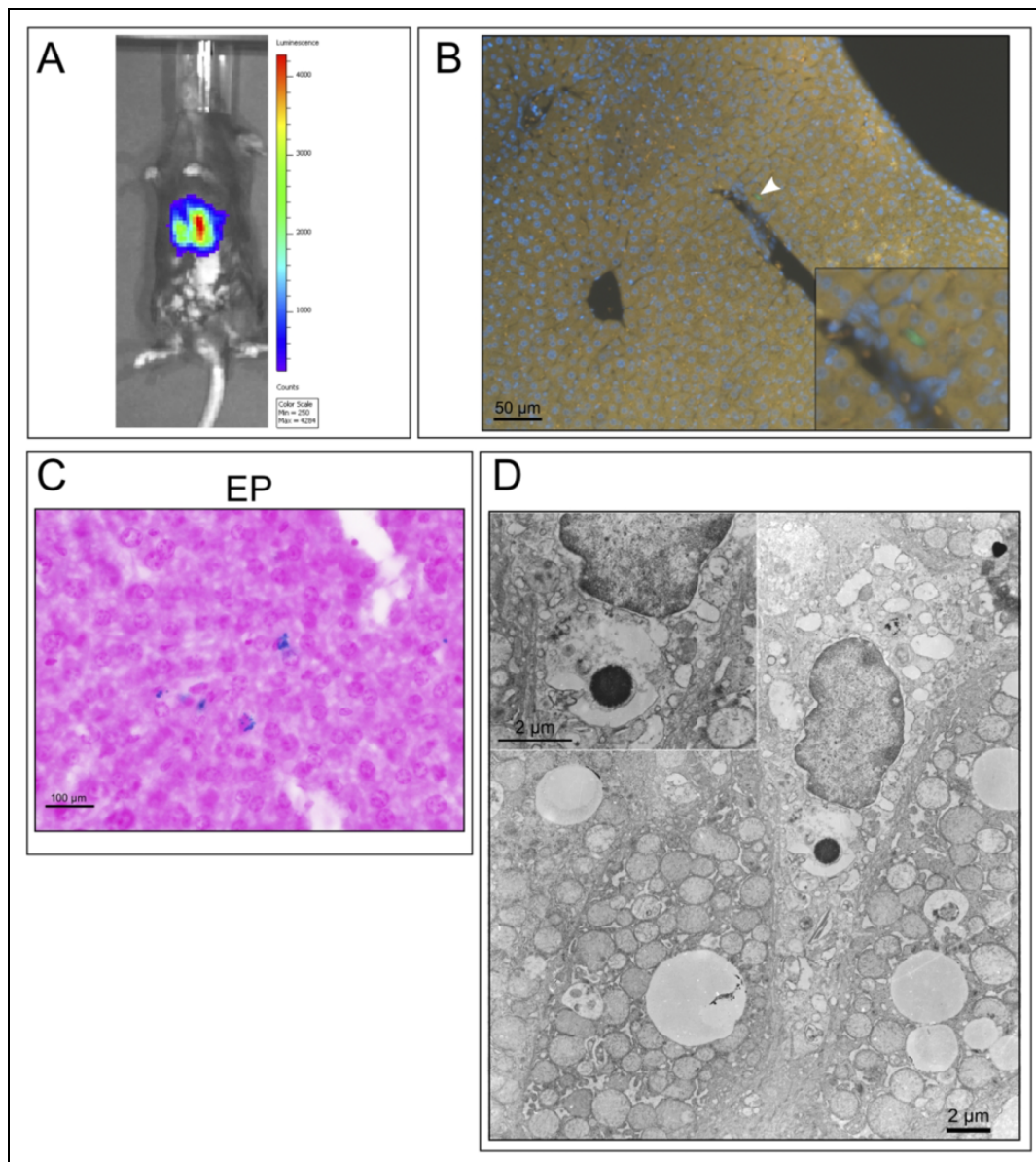


Figure 3. SPM-labeled human EP cells are readily detectable in mouse liver 3 h post-transplant. (A) In vivo imaging of luciferase-expressing EP cells 3 h post-transplant. (B) Fluorescent microscopy analysis of mouse liver section, from mouse shown in (A); arrowhead indicates transplanted hrGFP-expressing human EP (see inset for higher magnification); scale bar denotes 50 μm ; nuclei were stained with DAPI. (C) Prussian blue staining for the presence of iron, derived from mouse liver (shown in A and B) section; scale bar denotes 100 μm . (D) Electron microscopy from mouse liver (shown in A, B, and C) with iron particle labeling transplanted human EP cell; scale bars denote 2 μm . DAPI: 4',6-diamidino-2-phenylindole; EP: endoderm progenitor.

conclude the EP cells used here for transplantation (Fig. 3), and HP cells, are intrinsically activated toward EMT.

EMT is Active in EP and HP Cells Transplanted to the Quiescent Liver

Taking the above data collectively, we inferred that EMT could be observed in vivo in transplanted EP and HP cells. To test this possibility, we performed additional transplants to the undamaged/quiescent mouse liver, but this time carrying out analyses 24 h post-transplant. First, we used in vivo imaging to

confirm the presence of EP cells 24 h after delivery, and indeed observed a detectable signal (Fig. 5A). Next we analyzed the liver tissue from the same mouse with EM and observed a SPM-labeled EP cell that appears to have a leading edge protruding between hepatocytes (Fig. 5B), similar to that observed at 3 h (Fig. 3D), and consistent with active EMT. Therefore, at both 3 and 24 h after transplant, human EP cells show morphological characteristics consistent with active migration into the liver parenchyma through EMT.

We next asked if human HP cells also showed similar invasive characteristics during engraftment. As observed in

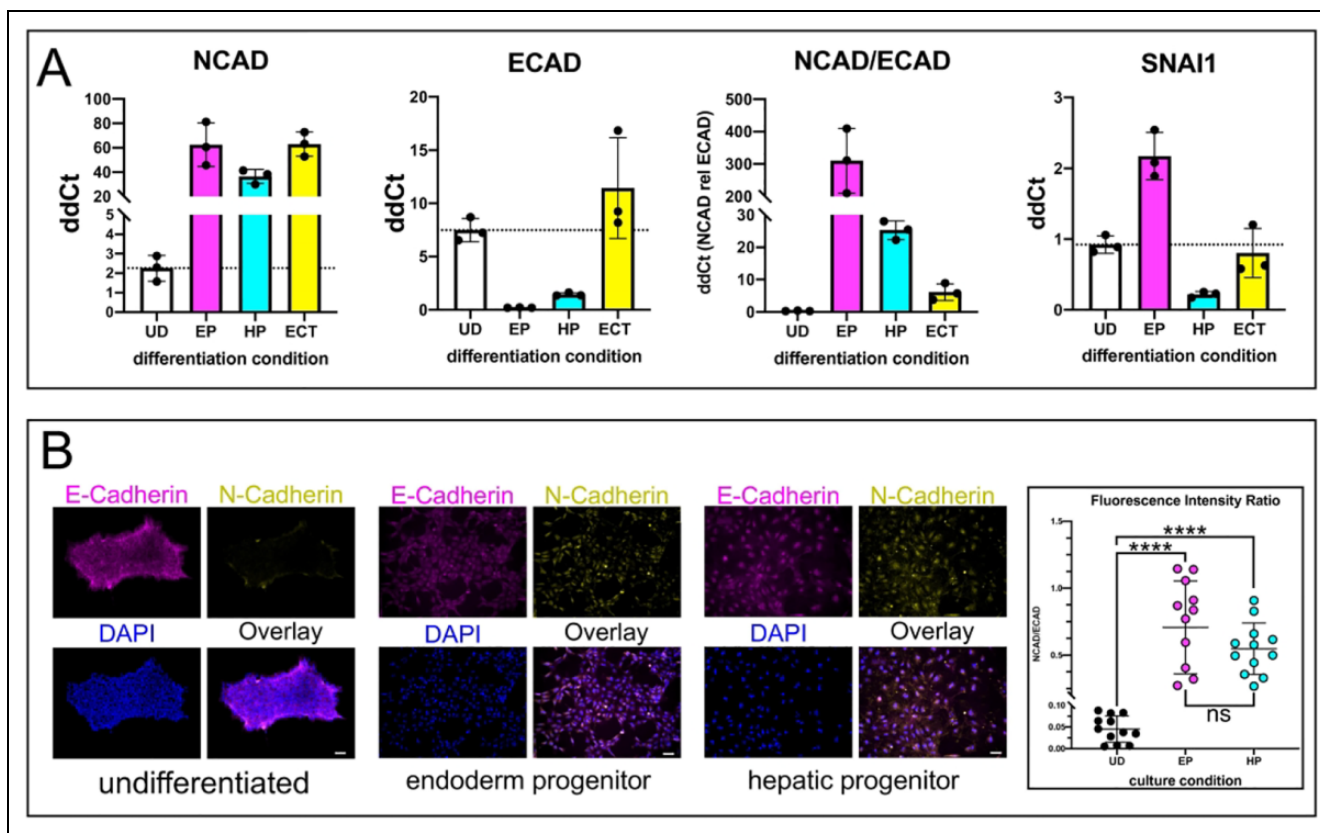


Figure 4. EMT is intrinsically activated in human EP and HP cells differentiated in vitro. (A) RT-qPCR analysis of RNA extracted from UD, EP, HP, and ECT cells displayed as delta-delta Ct values relative to HMBS “housekeeping gene product,” except in the case of N-Cadherin/E-Cadherin (NCAD/ECAD) where NCAD is shown relative to ECAD to determine the ratio of transcript abundances ($n = 3$ biological replicates shown as individual points, bars show mean, error bars show standard deviation). (B) Representative result of indirect immunofluorescence analyzed by fluorescent microscopy of human UD, EP, and HP cells stained with antibodies directed against E-Cadherin (magenta) or N-Cadherin (yellow), or stained with DAPI (blue), and each channel overlaid; scale bars denote 50 μm . Graph on the right shows fluorescent intensity ratios of N-Cadherin/E-Cadherin calculated per cell, with each point plotted representing a single cell ($ns =$ not significant; $****P < 0.001$ by Mann–Whitney and one-way ANOVA tests). ANOVA: analysis of variance; DAPI: 4',6-diamidino-2-phenylindole; EMT: epithelial-to-mesenchymal transition; EP: endoderm progenitor; HP: hepatic progenitor; UD: undifferentiated hESCs.

vivo with EP cells, SPM-labeled HP cells are identifiable using in vivo imaging (Fig. 5C), and in histological samples stained with Prussian blue (Fig. 5D). Also, using EM, we observed SPM-labeled HP cells engrafted in the quiescent liver 24 h post-transplant (Fig. 5E). Similar to EP cells, leading edges protruding between hepatocytes are readily apparent; thus, the morphology of engrafted HP cells is also consistent with an active EMT mechanism in vivo. Interestingly, HP cells in vivo appear to show more SPM particles per cell than EP cells, 24 h after transplant. This being the case we used these samples to perform immunolabeling to identify Vimentin in cells that are also positive for SPM particles, as Vimentin localized to the leading edge of invadopodia is a biomarker of active EMT²⁷. We found an engrafted HP cell with at least two SPMs, and inspection at higher magnification indicated positive Vimentin staining localized toward the cell periphery (Fig. 5F), further suggesting this HP cell had engrafted concurrent with activate EMT. Collectively these data support a model in which endoderm and HP cells, by

virtue of their smaller size compared to hepatocytes, and intrinsic bias toward EMT, can effectively migrate into the liver parenchyma quickly and efficiently post-delivery.

Discussion

The current study was undertaken to determine if the early engraftment mechanisms of human EP and HP cells are distinct from those observed for hepatocytes transplanted to the liver. We indeed found evidence supporting this notion, and specifically that these cells migrate through the space of Disse in a very rapid manner. This facilitates integration into the hepatic parenchyma with very little dwell time in the sinusoidal space. The EMT is active during this process, and it likely facilitates this prompt incorporation. Finally, the process presumably advances with simultaneous in vivo differentiation and MET to ultimately form epithelialized mature human hepatocytes. Determining how these

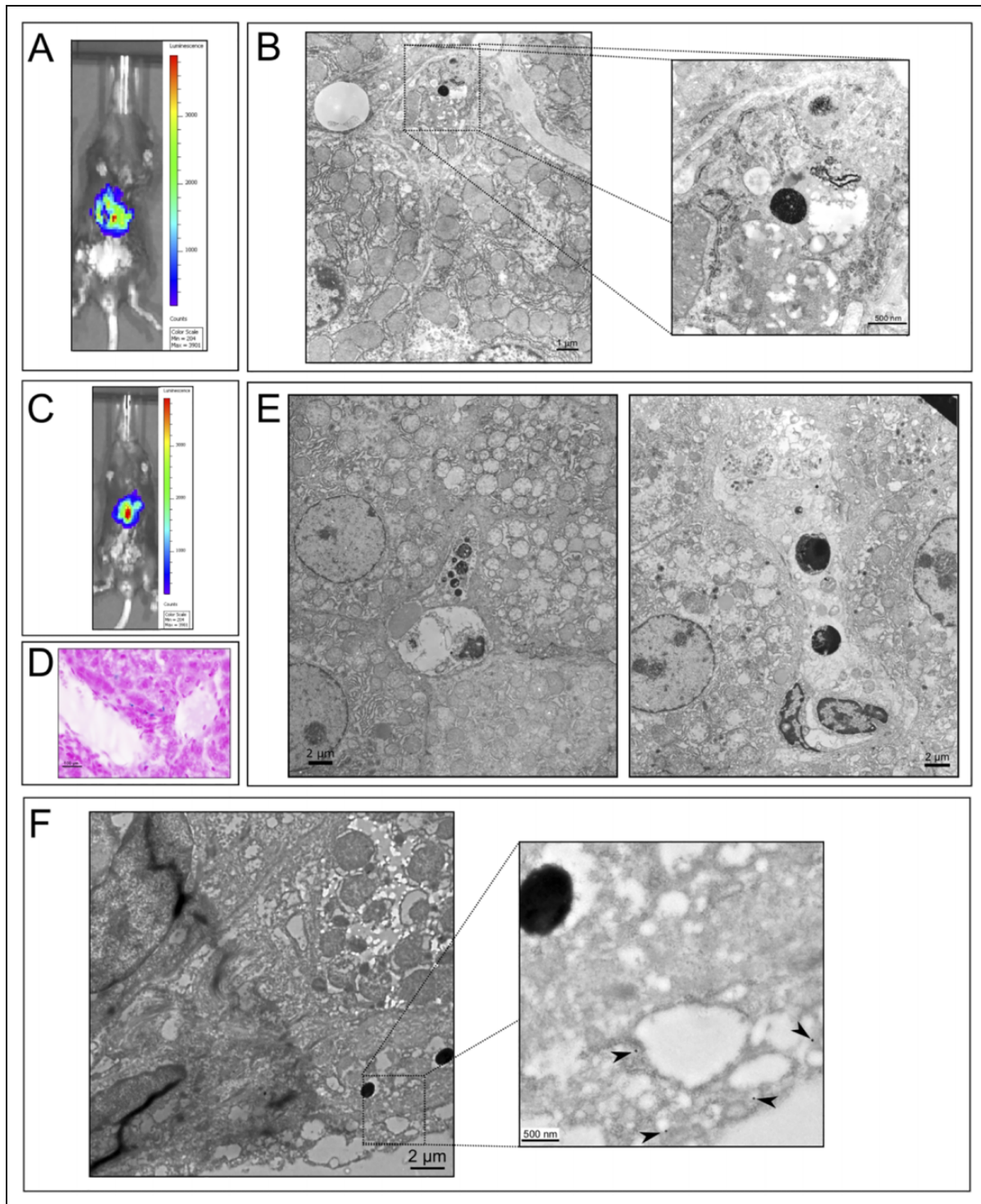


Figure 5. SPM-labeled human EP and HP cells are detectable in mouse liver 24 h post-transplant and exhibit features of EMT. (A) In vivo imaging of luciferase-expressing EP cells 24 h post-transplant. (B) Electron microscopy from mouse liver (shown in A) with iron particle-labeled transplanted human EP cells; scale bar denotes 1 μm on left image, with boxed region shown at higher magnification on right (scale bar denotes 500 nm). (C) In vivo imaging of luciferase-expressing HP cells 24 h post-transplant. (D) Prussian blue staining for the presence of iron, derived from mouse liver (shown in C) section; scale bar denotes 100 μm . (E) Electron microscopy from two independent lobes of mouse liver (shown in C and D) with iron particle-labeled transplanted human HP cells; scale bars denote 2 μm . (F) Electron microscopy from mouse liver (shown in C, D, and E) with iron particle-labeled transplanted human HP cells immunolabeled with Vimentin antibody and gold nanoparticle conjugate; scale bar denotes 2 μm in image on left, with boxed region shown at higher magnification on right (scale bar denotes 500 nm); arrowheads indicate gold particles. EMT: epithelial-to-mesenchymal transition; EP: endoderm progenitor; HP: hepatic progenitor.

convergent processes occur in vivo after transplantation will be a major focus and challenge going forward.

The implications of these findings are relevant for various types of progenitor cells' transplantation, in which one endeavors to regenerate the liver through adding hepatic biomass, such as described here with human EP and HP cells. Recent advances using amnion epithelial cells (AECs) indicate these could be efficacious^{28–31} and do not carry the pluripotency-associated safety risks observed with ES- and iPS-derived cells. Furthermore, the plasticity of AECs in the context of EMT^{32,33} is such that one might be able to activate this process immediately prior to or during transplantation to enhance engraftment. On the other hand, various other progenitor cell types have therapeutic effects independent of adding to or replacing the hepatic biomass. Ample evidence indicates various sources of mesenchymal stem/stromal cells^{34–36} and cardiac precursor cells^{37–39} therapeutic effects are mediated largely via secreted factors. The liver could potentially be a “safe harbor” for these cells, with little risk to the recipient, given these cells' small size and biases toward EMT. Collectively, the findings reported in this study have wide-ranging implications that span beyond cell transplantation for liver interventions and represent the early steps toward a paradigm shift in our collective understanding of progenitor cell utility.

Acknowledgment

We thank Zhixia Ding for technical support and assistance with EM.

Authors' Contributions

WSF, JHF, NL, and HLS conceived the overall study and performed the cell-based and animal-based portions of the experiments; IP and MM provided guidance, support, and training for in vivo imaging using the IVIS system; OAS and HLS performed sample prep and analysis of FFPE histology samples; VLP helped with experimental design, interpretation, and performed the sample preparation and EM experiments; and WSF wrote the paper. All authors contributed critical review of the manuscript, revisions, and have approved its submission.

Ethical Approval

This study was approved by the Institutional Animal Care and Use Committee of the University of Texas Medical Branch under protocol 1706040.

Statement of Human and Animal Rights

All experimental procedures involving animals were conducted in accordance with the institutional animal care guidelines at the University of Texas Medical Branch and approved by the Institutional Animal Care and Use Committee under protocol 1706040.

Statement of Informed Consent

No human subjects were involved in this study, therefore informed consent does not apply.


Declaration of Conflicting Interests

The author(s) declared no potential conflicts of interest with respect to the research, authorship, and/or publication of this article.

Funding

The author(s) disclosed receipt of the following financial support for the research, authorship, and/or publication of this article: The research was supported by the Moody Endowment Award (HLS), the NCATS CTSA KL2 Scholars Program Grant (KL2TR001441 to HLS) US National Institutes of Health grant HL082606-0 (JHF), the John Sealy Smith Endowment (JHF), the John L. Hearn Endowment (JHF), and Department of Surgery start-up funds (JHF).

ORCID iD

W. Samuel Fagg  <https://orcid.org/0000-0003-2909-1666>

References

- Jorns C, Ellis EC, Nowak G, Fischler B, Nemeth A, Strom SC, Ericzon BG. Hepatocyte transplantation for inherited metabolic diseases of the liver. *J Intern Med.* 2012;272(3):201–223.
- Strom SC, Bruzzone P, Cai H, Ellis E, Lehmann T, Mitamura K, Miki T. Hepatocyte transplantation: clinical experience and potential for future use. *Cell Transplant.* 2006;15(Suppl 1):S105–S110.
- Horslen SP, McCowan TC, Goertzen TC, Warkentin PI, Cai HB, Strom SC, Fox IJ. Isolated hepatocyte transplantation in an infant with a severe urea cycle disorder. *Pediatrics.* 2003; 111(6 Pt 1):1262–1267.
- Gupta S, Rajvanshi P, Sokhi R, Slehra S, Yam A, Kerr A, Novikoff PM. Entry and integration of transplanted hepatocytes in rat liver plates occur by disruption of hepatic sinusoidal endothelium. *Hepatology.* 1999;29(2):509–519.
- Baccarani U, Adani GL, Sanna A, Avellini C, Sainz-Barriga M, Lorenzin D, Montanaro D, Gasparini D, Risaliti A, Donini A, Bresadola F. Portal vein thrombosis after intraportal hepatocytes transplantation in a liver transplant recipient. *Transpl Int.* 2005;18(6):750–754.
- Stéphenne X, Najimi M, Smets F, Reding R, de Ville de Goyet J, Sokal EM. Cryopreserved liver cell transplantation controls ornithine transcarbamylase deficient patient while awaiting liver transplantation. *Am J Transplant.* 2005;5(8):2058–2061.
- Habibullah CM, Syed IH, Qamar A, Taher-Uz Z. Human fetal hepatocyte transplantation in patients with fulminant hepatic failure. *Transplantation.* 1994;58(8):951–952.
- Tsolaki E, Yannaki E. Stem cell-based regenerative opportunities for the liver: state of the art and beyond. *World J Gastroenterol.* 2015;21(43):12334–12350.
- Oertel M, Shafritz DA. Stem cells, cell transplantation and liver repopulation. *Biochim Biophys Acta.* 2008;1782(2):61–74.
- Strom SC, Gramignoli R. Human amnion epithelial cells expressing HLA-G as novel cell-based treatment for liver disease. *Hum Immunol.* 2016;77(9):734–739.
- Azuma H, Paulk N, Ranade A, Dorrell C, Al-Dhalimy M, Ellis E, Strom S, Kay MA, Finegold M, Grompe M. Robust expansion of human hepatocytes in Fah^{-/-}/Rag2^{-/-}/Il2rg^{-/-} mice. *Nat Biotechnol.* 2007;25(8):903–910.

12. Liu H, Kim Y, Sharkis S, Marchionni L, Jang YY. In vivo liver regeneration potential of human induced pluripotent stem cells from diverse origins. *Sci Transl Med*. 2011;3(82):82ra39.
13. Loh KM, Ang LT, Zhang J, Kumar V, Ang J, Auyeong JQ, Lee KL, Choo SH, Lim CY, Nichane M, Tan J, et al. Efficient endoderm induction from human pluripotent stem cells by logically directing signals controlling lineage bifurcations. *Cell Stem Cell*. 2014;14(2):237–252.
14. Fair JH, Cairns BA, Lapaglia MA, Caballero M, Pleasant WA, Hatada S, Kim HS, Gui T, Pevny L, Meyer AA, Stafford DW, et al. Correction of factor IX deficiency in mice by embryonic stem cells differentiated in vitro. *Proc Natl Acad Sci U S A*. 2005;102(8):2958–2963.
15. Fagg WS, Liu N, Yang MJ, Cheng K, Chung E, Kim JS, Wu G, Fair J. Magnetic targeting of stem cell derivatives enhances hepatic engraftment into structurally normal liver. *Cell Transplant*. 2017;26(12):1868–1877.
16. Turovets N, Fair J, West R, Ostrowska A, Semechkin R, Janus J, Cui L, Agapov V, Turovets I, Semechkin A, Csete M, et al. Derivation of high-purity definitive endoderm from human parthenogenetic stem cells using an in vitro analog of the primitive streak. *Cell Transplant*. 2012;21(1):217–234.
17. Robb L, Tam PP. Gastrula organiser and embryonic patterning in the mouse. *Semin Cell Dev Biol*. 2004;15(5):543–554.
18. Hay ED. The mesenchymal cell, its role in the embryo, and the remarkable signaling mechanisms that create it. *Dev Dyn*. 2005;233(3):706–720.
19. Li Q, Hutchins AP, Chen Y, Li S, Shan Y, Liao B, Zheng D, Shi X, Li Y, Chan WY, Pan G, et al. A sequential EMT-MET mechanism drives the differentiation of human embryonic stem cells towards hepatocytes. *Nat Commun*. 2017;8(1):15166.
20. Hatada S, Subramanian A, Mandefro B, Ren S, Kim HW, Tang J, Funari V, Baloh RH, Sareen D, Arumugaswami V, Svendsen CN. Low-dose irradiation enhances gene targeting in human pluripotent stem cells. *Stem Cells Transl Med*. 2015;4(9):998–1010.
21. Loh KM, Chen A, Koh PW, Deng TZ, Sinha R, Tsai JM, Barkal AA, Shen KY, Jain R, Morganti RM, Shyh-Chang N, et al. Mapping the pairwise choices leading from pluripotency to human bone, heart, and other mesoderm cell types. *Cell*. 2016;166(2):451–467.
22. Smukler SR, Runciman SB, Xu S, van der Kooy D. Embryonic stem cells assume a primitive neural stem cell fate in the absence of extrinsic influences. *J Cell Biol*. 2006;172(1):79–90.
23. Tajbakhsh J, Gertych A, Fagg WS, Hatada S, Fair JH. Early in vitro differentiation of mouse definitive endoderm is not correlated with progressive maturation of nuclear DNA methylation patterns. *PLoS One*. 2011;6(7):e21861.
24. Fagg WS, Liu N, Fair JH, Shiue L, Katzman S, Donohue JP, Ares M, Jr. Autogenous cross-regulation of Quaking mRNA processing and translation balances Quaking functions in splicing and translation. *Genes Dev*. 2017;31(18):1894–1909.
25. Meguro R, Asano Y, Odagiri S, Li C, Iwatsuki H, Shoumura K. Nonheme-iron histochemistry for light and electron microscopy: a historical, theoretical and technical review. *Arch Histol Cytol*. 2007;70(1):1–19.
26. Tanimizu N, Miyajima A. Molecular mechanism of liver development and regeneration. *Int Rev Cytol*. 2007;259:1–48.
27. Schoumacher M, Goldman RD, Louvard D, Vignjevic DM. Actin, microtubules, and vimentin intermediate filaments cooperate for elongation of invadopodia. *J Cell Biol*. 2010;189(3):541–556.
28. Marongiu F, Gramignoli R, Dorko K, Miki T, Ranade AR, Paola Serra M, Doratiotto S, Sini M, Sharma S, Mitamura K, Sellaro TL, et al. Hepatic differentiation of amniotic epithelial cells. *Hepatology*. 2011;53(5):1719–1729.
29. Marongiu M, Serra MP, Contini A, Sini M, Strom SC, Laconi E, Marongiu F. Rat-derived amniotic epithelial cells differentiate into mature hepatocytes in vivo with no evidence of cell fusion. *Stem Cells Dev*. 2015;24(12):1429–1435.
30. Skvorak KJ, Dorko K, Marongiu F, Tahan V, Hansel MC, Gramignoli R, Gibson KM, Strom SC. Placental stem cell correction of murine intermediate maple syrup urine disease. *Hepatology*. 2013;57(3):1017–1023.
31. Strom SC, Skvorak K, Gramignoli R, Marongiu F, Miki T. Translation of amnion stem cells to the clinic. *Stem Cells Dev*. 2013;22(Suppl 1):96–102.
32. Richardson L, Menon R. Proliferative, migratory, and transition properties reveal metastate of human amnion cells. *Am J Pathol*. 2018;188(9):2004–2015.
33. Richardson LS, Taylor RN, Menon R. Reversible EMT and MET mediate amnion remodeling during pregnancy and labor. *Sci Signal*. 2020;13(618):eaay1486.
34. Lazzarini E, Balbi C, Altieri P, Pfeffer U, Gambini E, Canepa M, Varesio L, Bosco MC, Coviello D, Pompilio G, Brunelli C, et al. The human amniotic fluid stem cell secretome effectively counteracts doxorubicin-induced cardiotoxicity. *Sci Rep*. 2016;6(1):29994.
35. Spitzhorn LS, Rahman MS, Schwindt L, Ho HT, Wruck W, Bohndorf M, Wehrmeyer S, Ncube A, Beyer I, Hagenbeck C, Balan P, et al. Isolation and molecular characterization of amniotic fluid-derived mesenchymal stem cells obtained from caesarean sections. *Stem Cells Int*. 2017;2017:5932706.
36. Madrigal M, Rao KS, Riordan NH. A review of therapeutic effects of mesenchymal stem cell secretions and induction of secretory modification by different culture methods. *J Transl Med*. 2014;12:260.
37. Cheng K, Malliaras K, Smith RR, Shen D, Sun B, Blusztajn A, Xie Y, Ibrahim A, Aminzadeh MA, Liu W, Li TS, et al. Human cardiosphere-derived cells from advanced heart failure patients exhibit augmented functional potency in myocardial repair. *JACC Heart Fail*. 2014;2(1):49–61.
38. Malliaras K, Li TS, Luthringer D, Terrovitis J, Cheng K, Chakravarty T, Galang G, Zhang Y, Schoenhoff F, Van Eyk J, Marbán L, et al. Safety and efficacy of allogeneic cell therapy in infarcted rats transplanted with mismatched cardiosphere-derived cells. *Circulation*. 2012;125(1):100–112.
39. Rogers RG, Fournier M, Sanchez L, Ibrahim AG, Aminzadeh MA, Lewis MI, Marbán E. Disease-modifying bioactivity of intravenous cardiosphere-derived cells and exosomes in mdx mice. *JCI Insight*. 2019;4(7):e130202.